THE JOURNAL OF PHYSICAL CHEMISTRY LETTERS
A JOURNAL OF THE AMERICAN CHEMICAL SOCIETY

pubs.acs.org/JPCL
Letter

Electrochemical Lithiation and Delithiation of Amorphous Nonstoichiometric Silicon Oxide Thin-Film Electrode Studied by *Operando* X-ray Photoelectron Spectroscopy

Tsukasa Iwama, Ryosuke Sugimoto, Raimu Endo, Tsuyoshi Ohnishi, Masakazu Haruta, Takayuki Doi, and Takuya Masuda*

Cite This: *J. Phys. Chem. Lett.* 2026, 17, 2181−2190

ABSTRACT: Electrochemical lithiation/delithiation of a nonstoichiometric silicon oxide (SiO_x) thin-film electrode on a $Li_{6.6}La_3Zr_{1.6}Ta_{0.4}O_{12}$ were analyzed using *operando* X-ray photoelectron spectroscopy (XPS). At the pristine SiO_x surface, bulk Si and SiO_x peaks were observed and remained unchanged in the capacity density from 0 to ∼1300 mAh g_{Si}^{-1}. At the capacity density of ∼1400 mAh g_{Si}^{-1}, however, new peaks corresponding to $Li_{\sim 2.0}Si$ and Li silicates appeared simultaneously with a substantial decrease in the bulk Si and SiO_x peaks. These results imply that, in the initial stage, lithiation of SiO_x occurred at the $SiO_x/Li_{6.6}La_3Zr_{1.6}Ta_{0.4}O_{12}$ interface to form Li_ySi and Li silicates, which was beyond the probing depth of XPS. Subsequently, lithiation gradually propagated into the bulk and approached the probing depth of XPS as the composition reached $Li_{\sim 2.0}Si$, thereby elongating the ion conductive pathway. Thereafter, the position of the Li_ySi peak reversibly responded to the state of charge because lithiation/delithiation occurred uniformly across the SiO_x thin film.

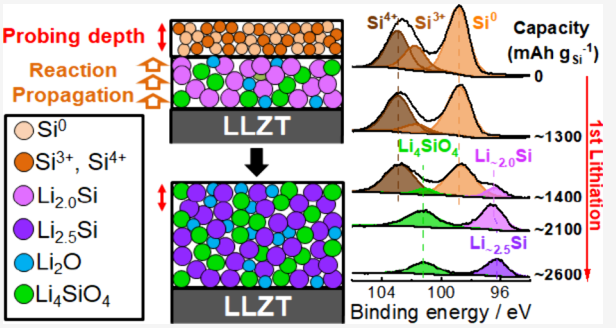

Pure Si anodes have an excellent theoretical capacity density of 4200 mAh g^{-1} corresponding to $Li_{4.4}Si$ (3579 mAh g^{-1} corresponding to $Li_{3.75}Si$ at room temperature).[1−6] However, they undergo considerable (∼300%) volume change initiated by crystal structure changes during electrochemical lithiation/delithiation cycles, which causes mechanical failure of the composite electrode, leading to poor cycle performance.[7−11] Nonstoichiometric silicon oxide (SiO_x) shows very large irreversible capacity loss in the initial cycle because part of electrochemically inserted Li is consumed for the formation of electrochemically inactive species, such as Li_2O and Li silicates.[12−15] However, SiO_x anodes demonstrate significantly improved cycle performance as compared to that of pure Si anodes.[16−20]

To date, electrochemical lithiation/delithiation mechanisms of SiO_x electrodes have been explored by various research groups.[12−26] Kim et al. used *ex-situ* solid-state nuclear magnetic resonance (NMR) to examine silicon monoxide (SiO) in a liquid-based electrolyte. They confirmed reversible lithiation and delithiation of Si domains, to form amorphous lithium silicide (*a*-Li_ySi), as well as the irreversible lithiation of SiO_2 domains to form highly resistive species such as Li silicates and Li_2O.[14] Takezawa et al. investigated the morphology and elemental composition of a SiO_x film electrode after repeated electrochemical cycles in a liquid-based electrolyte, using scanning electron microscopy (SEM) and electron probe microanalysis (EPMA). They proposed that the improved cycle performance of the SiO_x film electrode originates from the formation of Li silicates and Li_2O which act as buffer layers against the volume change of Li_ySi.[20]

In our previous study, electrochemical lithiation/delithiation reaction of an *a*-Si thin-film electrode sputter-deposited on a $Li_{6.6}La_3Zr_{1.6}Ta_{0.4}O_{12}$ (LLZT) solid electrolyte in a Si/LLZT/Li configuration was analyzed by *operando* X-ray photoelectron spectroscopy (XPS).[27] Although XPS measurements were performed at the *a*-Si surface opposite the Si/LLZT interface, upon lithiation, the Si 2p peak drastically shifted to a lower binding energy due to the formation of *a*-Li_ySi, indicating a spatially uniform distribution of lithiation reaction across the entire electrode. Then, as the capacity increased, the Li_ySi peak monotonically shifted to a lower binding energy. When the lithiation stopped at a capacity of 2200 mAh g^{-1}, the Li_ySi peak monotonically shifted to a higher binding energy throughout subsequent delithiation. When Li was inserted into the Li_ySi up

Received: December 26, 2025
Revised: January 29, 2026
Accepted: January 30, 2026
Published: February 4, 2026

https://doi.org/10.1021/acs.jpclett.5c04065
J. Phys. Chem. Lett. 2026, 17, 2181−2190

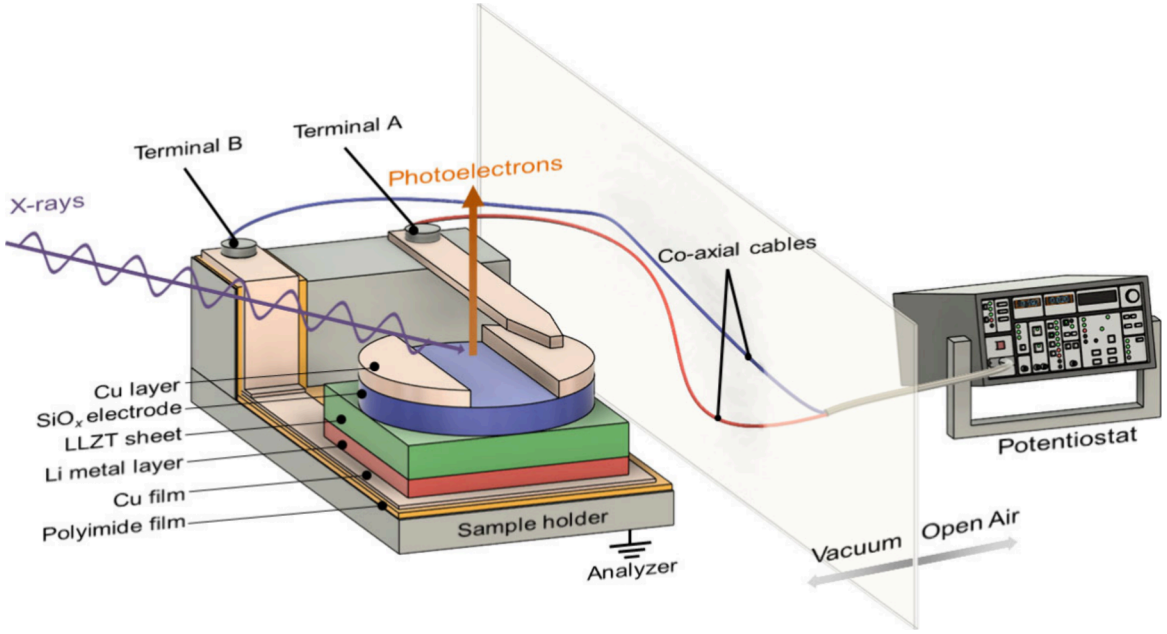

Figure 1. Schematic illustration of a Cu/SiO_x/LLZT/Li ASS half-cell mounted onto a sample holder connected to a potentiostat for *operando* XPS measurements.

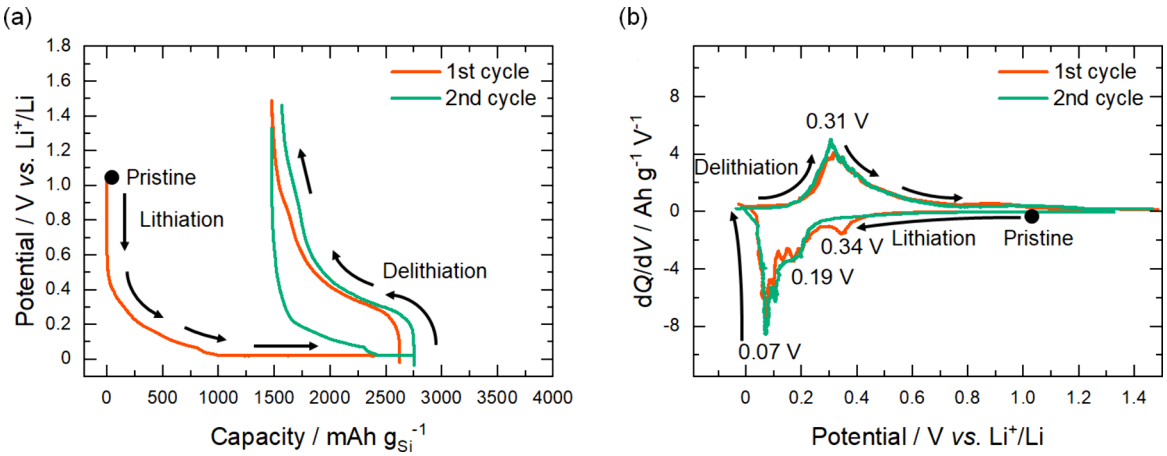

Figure 2. (a) Potential profiles and (b) generated dQ/dV curves during the first and second lithiation/delithiation processes of the *a*-SiO_x thin-film electrode in the Cu/SiO_x/LLZT/Li ASS half-cell. Specific capacity was normalized by the weight of deposited Si in the *a*-SiO_x thin-film electrode.

to a capacity of 3400 mAh g^{-1}, where crystalline-$Li_{3.75}Si$ (*c*-$Li_{3.75}Si$) and *a*-Li_ySi coexisted, however, the Li_ySi peak drastically shifted to a higher binding energy in the region of Li content y = 2.0−1.6 in the subsequent delithiation due to the phase transition from the *c*-$Li_{3.75}Si$ to *a*-Li_ySi.[27]

In the present study, we investigated the mechanism of electrochemical lithiation/delithiation of a sputter-deposited *a*-SiO_x thin-film electrode on a LLZT solid electrolyte using *operando* XPS. Analysis based on the correlation between Li_ySi peak positions and Li content y, as reported in our previous study,[27] enabled the identification of Li_ySi phases at each stage. This revealed that, in *a*-SiO_x, the reaction initially occurs only in the vicinity of the SiO_x/LLZT interface, and subsequently propagates throughout the entire thin film as ion conductive pathways of $Li_{\sim 2.0}Si$ are formed. Thereafter, electrochemical lithiation/delithiation reversibly occurs while maintaining a spatially uniform Li composition across the thin film. In addition, electrochemical lithiation of Li_ySi was found to spontaneously cease at lower Li content as compared to pure Si electrode probably due to the formation of highly resistive byproducts such as Li_2O and Li silicates.

An *a*-SiO_x thin film with a diameter of 10 mm and thickness of around 100 nm was deposited on a LLZT sheet (10 mm × 10 mm × 500 μm; Toshima Manufacturing Co., Ltd.) by radio frequency magnetron sputtering with Ar/O_2 gas mixtures.[16,18] Then, a Cu current collector was deposited onto the SiO_x layer by direct current sputtering, with a 10 mm × 4 mm central area masked by a stainless-steel stencil plate to leave an uncoated SiO_x region for XPS measurements. Finally, a Li metal layer with a thickness of around 1.5 μm was thermally evaporated onto the opposite surface of the LLZT sheet to yield a Cu/SiO_x/LLZT/Li all-solid-state (ASS) half-cell, as shown in Figure 1.

Electrochemical lithiation/delithiation and XPS measurements were performed simultaneously using an *operando* XPS system.[27−29] Lithiation of the SiO_x thin-film electrode of the ASS half-cell was conducted in constant-current (CC)−constant-voltage (CV) mode: a constant current of 4.9 μA

https://doi.org/10.1021/acs.jpclett.5c04065
J. Phys. Chem. Lett. 2026, 17, 2181−2190

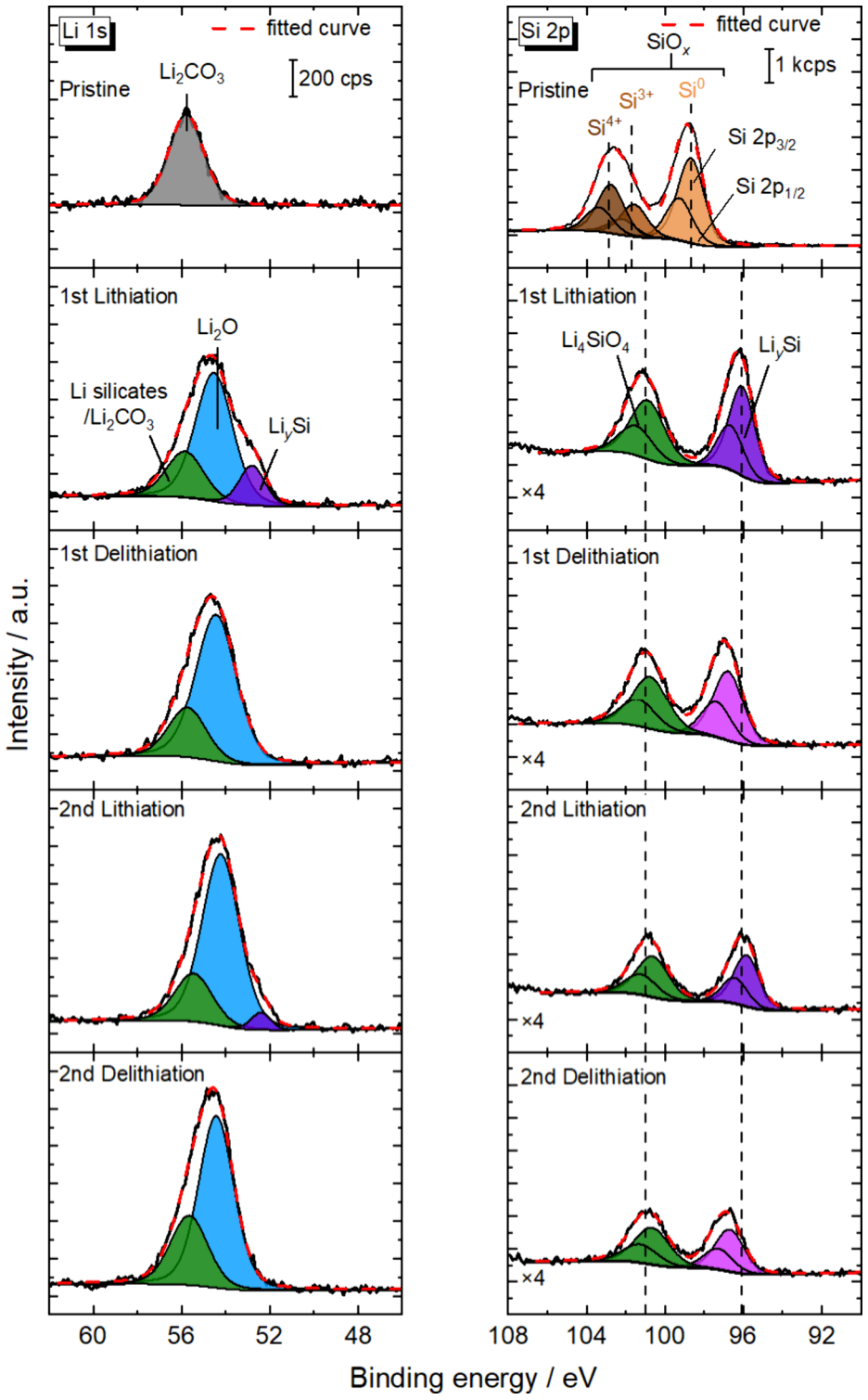

Figure 3. Li 1s and Si 2p photoelectron spectra of the *a*-SiO_x thin-film electrode in a Cu/SiO_x/LLZT/Li ASS half-cell after the first and second lithiation and delithiation.

cm^{-2} (~0.134 C, 1 C = 3579 mA g^{-1} for $Li_{3.75}Si$) was applied until the cell voltage reached 0.02 V (109 min), followed by maintaining 0.02 V until the current density decreased to 0.49 μA cm^{-2} (546 min). Delithiation was carried out with a constant-current (CC) mode: a constant current of 2.45 μA cm^{-2} (~0.067 C) was applied until the cell voltage reached 1.5 V (285 min). Subsequent lithiation/delithiation cycles followed the same procedure, but the current densities for CC and CV for lithiation were set to half of those for the first lithiation.

Figure 2 (a) shows the lithiation/delithiation potential profiles obtained for the ASS half-cell. The capacity densities are given in mAh g_{Si}^{-1} based on the weight of Si in the *a*-SiO_x thin-film electrode. It is noted that the composition of *a*-SiO_x in the present study was determined to be *a*-$SiO_{0.5}$ (see below). The first lithiation and delithiation capacity densities

https://doi.org/10.1021/acs.jpclett.5c04065
J. Phys. Chem. Lett. 2026, 17, 2181−2190

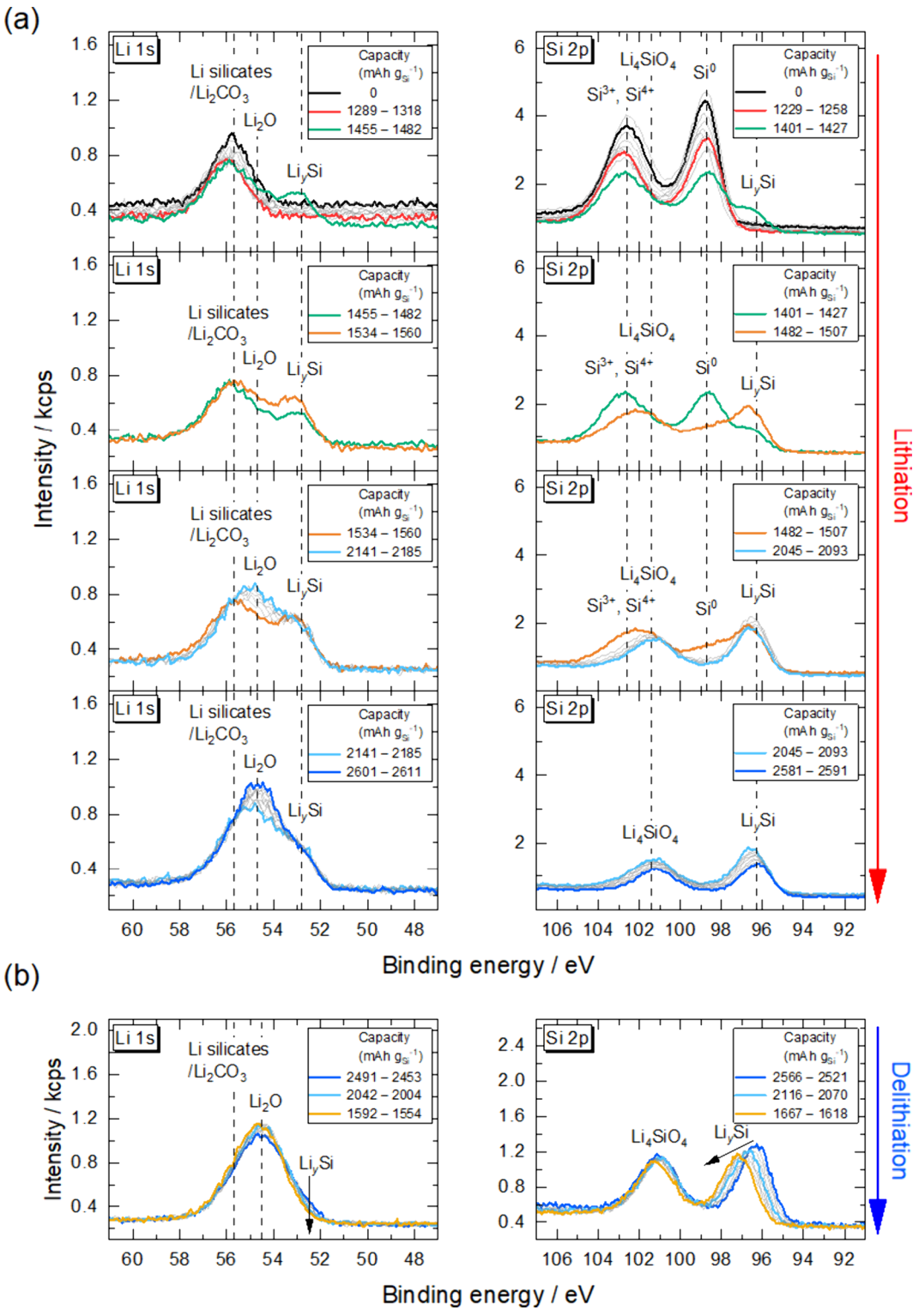

Figure 4. Li 1s and Si 2p photoelectron spectra of the *a*-SiO_x thin-film electrode in a Cu/SiO_x/LLZT/Li ASS half-cell during the first (a) lithiation and (b) delithiation.

were 2625 and 1148 mAh g_{Si}^{-1}, respectively. The initial Coulombic efficiency of the SiO_x thin film, 43.7%, was much lower than those of previous reports on pure Si thin-film electrode in both liquid-electrolyte-based[3,30,31] and all-solid-state configurations[27,29,32,33] but in reasonable agreement with that of SiO_x in a liquid-based electrolyte.[23] In the second cycle, the lithiation and delithiation capacity densities were 1276 and 1185 mAh g_{Si}^{-1}, respectively, with a Coulombic efficiency of 92.8%.

Figure 2 (b) shows negative and positive dQ/dV curves obtained by differentiating the smoothed potential profiles during lithiation and delithiation, respectively. In the negative dQ/dV curve during the first lithiation, three peaks observed at around 0.34, 0.19, and 0.07 V were attributed to lithiation of *a*-

https://doi.org/10.1021/acs.jpclett.5c04065
J. Phys. Chem. Lett. 2026, 17, 2181−2190

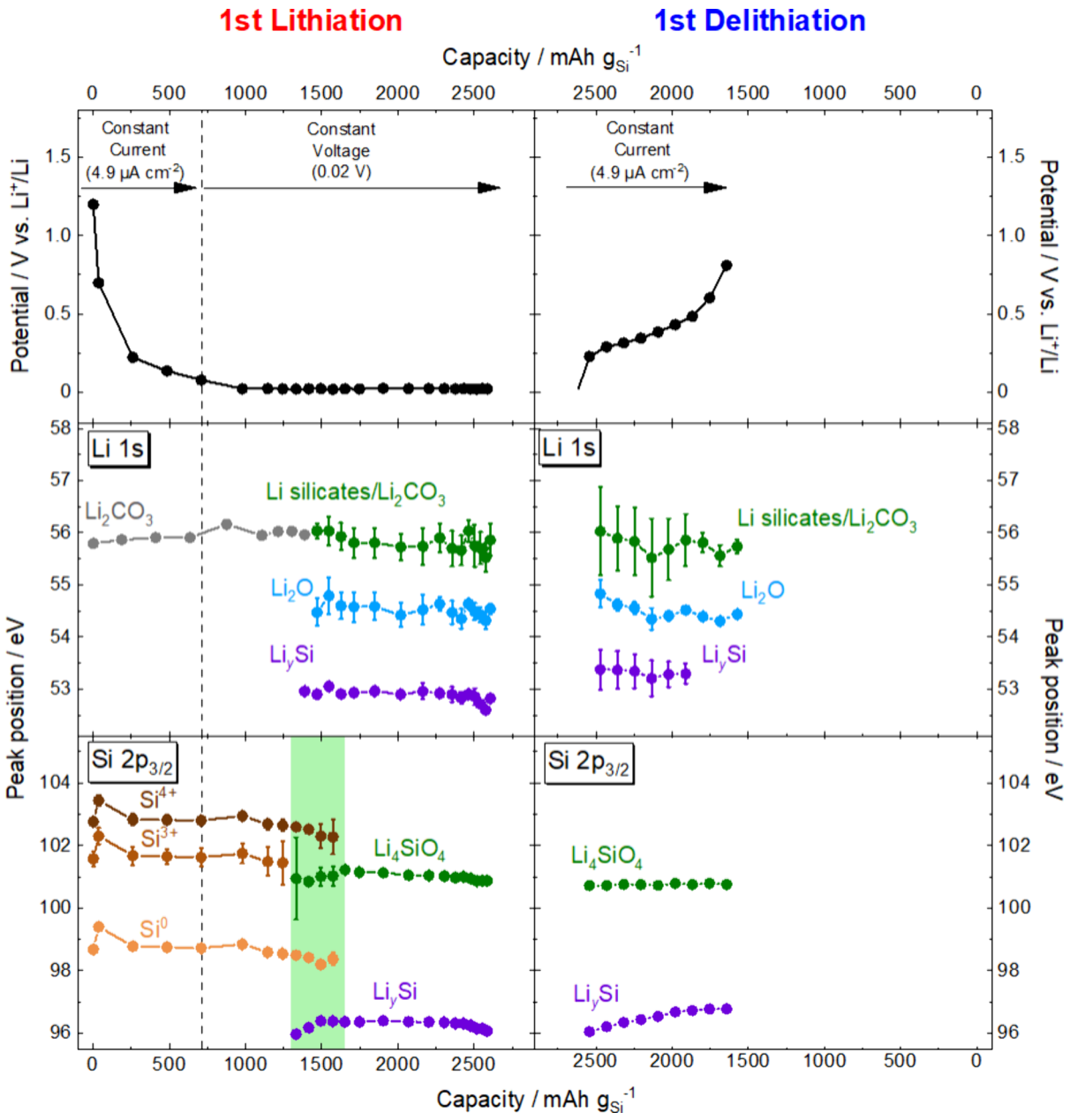

Figure 5. Potential profiles and Li 1s and Si $2p_{3/2}$ peak positions of each chemical species as a function of capacity density during the first lithiation and delithiation. The green area in Si $2p_{3/2}$ regions represent the region where Si^0, Si^{3+}, Si^{4+}, Li_4SiO_4, and Li_ySi coexist.

SiO_x to form Li_2O and Li silicates,[13,14,19] lithiation of Si to form Li-poor *a*-Li_ySi,[19] and lithiation of the Li-poor *a*-Li_ySi to form Li-rich *a*-Li_ySi,[13,19,21] respectively. The positive dQ/dV curve during the first delithiation showed a broad peak at around 0.31 V corresponding to delithiation of Li-rich *a*-Li_ySi.[19]

In the second lithiation, the negative peak corresponding to lithiation of SiO_x observed at around 0.34 V in the first lithiation completely disappeared, confirming elimination of SiO_x to form Li_2O and Li silicates in the first lithiation.[13,14,19] Except for this point, the positive and negative dQ/dV curves remained almost unchanged thereafter, indicating reversible lithiation/delithiation processes.

Figure 3 shows the Li 1s and Si 2p photoelectron spectra of the *a*-SiO_x thin-film electrode after the first and second lithiation/delithiation processes. In the pristine state, Si $2p_{3/2}$ peaks observed at around 98.7 eV were attributed to the bulk Si (Si^0), while a broad peak observed at around 99.7−102.7 eV was deconvoluted into two peaks of Si_2O_3 (Si^{3+}) at 101.7 eV and SiO_2 (Si^{4+}) at 102.7 eV as a result of curve fitting analysis with the Voigt function, as shown in Figure S1.[17,23,34−36] Although the curve fitting analysis was performed based on an assumption that the Si 2p spectra in SiO_x were composed of five species with the oxidation states Si^0, Si_2O (Si^{1+}), SiO (Si^{2+}), Si_2O_3 (Si^{3+}), and SiO_2 (Si^{4+}), the best fit was obtained with three pairs of peaks consisting of Si^0, Si^{3+} and Si^{4+} species. The details for the curve fitting analysis in the Si 2p region are described in the Supporting Information.

The composition of SiO_x in the pristine state was estimated to be $SiO_{0.87}$, $SiO_{0.50}$ and $SiO_{0.53}$ by XPS using an Al Kα source, HAXPES using a Cr Kα source, and SEM-EDS analysis, respectively, as shown in Figure S1 and Table S1 in the

https://doi.org/10.1021/acs.jpclett.5c04065
J. Phys. Chem. Lett. 2026, 17, 2181−2190

Supporting Information. Even if the samples were handled only in a vacuum chamber or Ar-filled glovebox, the growth of Si oxides still occurs.[29] In addition, such an outermost oxide layer becomes more dominant in photoelectron spectra measured using an Al Kα source due to its relatively high surface sensitivity. On the other hand, techniques with greater information depth, such as HAXPES and SEM-EDS, are considered to provide results that reflect the composition of the entire SiO_x layer. Thus, the value x in SiO_x used in this study is most likely ~0.5.

It is noted that the Si^0 peak was observed at a binding energy slightly lower than those of a-Si thin-film electrode in the pristine state (99.1 eV)[27] and commercially available pure Si (99.2 eV).[37] Based on the correlation between the position of Si $2p_{3/2}$ peak and Li content y in Li_ySi in Table S2 and Figure S2 in the Supporting Information,[27] the peak at 98.7 eV was attributed to $Li_{0-0.02}Si$. In addition, a peak corresponding to Li_2CO_3 was observed in the Li 1s and C 1s regions in the pristine state.[38] These results suggest that a small amount of Li species introduced as impurities during the sample preparation procedure can be inserted into Si^0 of the SiO_x thin film to form slightly lithiated species, $Li_{0-0.02}Si$. Subsequently, part of $Li_{0-0.02}Si$ further reacted with residual gases such as O_2 and CO_2 present in the vacuum chamber.

After the first lithiation, in addition to the Li_2CO_3 peak at 55.9 eV which cannot be deconvoluted from Li silicates, species assignable to Li_ySi and Li_2O were observed at around 52.8 and 54.5 eV in the Li 1s region, respectively. In the Si 2p region, a Si $2p_{3/2}$ peak corresponding to $Li_{0-0.02}Si$ shifted to a lower binding energy up to 96.1 eV which is equivalent to $Li_{2.53}Si$ based on the correlation in Figure S2,[27] confirming the increase in Li content.[28,39] In addition, the peaks corresponding to Si^{3+} species at around 101.7 eV and Si^{4+} species at around 102.7 eV merged into a peak at around 100.9 eV due to the formation of Li_4SiO_4.[23,29,39−41] It is worth noting that the intensities of Si 2p peaks became much smaller than those of the pristine state because the atomic density of Si decreased due to the lithiation. Moreover, photoelectrons ejected from Li_ySi were significantly attenuated by the topmost layer composed of Li_2O, Li_2CO_3, and Li_4SiO_4. Based on an assumption that all the electrochemical charge was consumed for the lithiation of Si atoms contained in the a-SiO_x thin film, $Li_{2.75}Si$ should be formed during the first lithiation with the capacity density of 2625 mAh g_{Si}^{-1}, and thus around 8% of Li ions were consumed for the formation of Li_4SiO_4 and Li_2O.

After the first delithiation, the Li_ySi peak at around 52.8 eV disappeared from the Li 1s region. Moreover, the shift of the Li_ySi peak from 96.1 to 97.0 eV in the Si 2p region confirms the decrease of Li content from $Li_{2.53}Si$ to $Li_{1.20}Si$ using the correlation in Figure S3.[27,39] In contrast, the Li_2O and Li_2CO_3/Li silicates peaks in the Li 1s region and the Li_4SiO_4 peak in the Si 2p region remained unchanged, indicating their very high resistivity. At this stage, highly resistive species, such as newly formed Li_4SiO_4 and Li_2O and initially present Li_2CO_3, as well as $Li_{1.20}Si$, remained on the anode. The amount of Li consumed in the formation of Li_4SiO_4 and Li_2O corresponds to 8% of the initial charge capacity, which is equivalent to 203 mAh g_{Si}^{-1}. In addition, the amount of Li trapped in $Li_{1.20}Si$ corresponds to 1143 mAh g_{Si}^{-1}, making the total 1346 mAh g_{Si}^{-1}, which is slightly less than the irreversible capacity for the first lithiation/delithiation cycle of 1477 mAh g_{Si}^{-1}, as shown in Figure 2(a). The origin of the remaining irreversible capacity of 131 mAh g_{Si}^{-1} may be due to a possible error of about 5−10% in the correlation between the Si 2p peak position corresponding to Li_ySi and Li content y, or to the presence of O-rich SiO_x at vicinity of the SiO_x/LLZT interface, which leads to the formation of a larger amount of Li_4SiO_4 and Li_2O.

In the second cycle, the Li_ySi peaks in the Li 1s and Si 2p regions quasi-reversibly responded to the electrochemical lithiation/delithiation with the remaining spectral features related to Li_2O, Li_2CO_3, and Li_4SiO_4 almost unchanged.

To elucidate the electrochemical lithiation/delithiation mechanism of the a-SiO_x thin-film electrode, the spectral changes during the first and second cycles were monitored in a stepwise manner. Figure 4 shows the time course of photoelectron spectra during the first lithiation and delithiation. The peak positions of each chemical species in the Li 1s and Si $2p_{3/2}$ regions were plotted as a function of capacity density as shown in Figure 5. As described above, a peak corresponding to Li_2CO_3 was observed at around 55.9 eV in the Li 1s region in a pristine state. In the Si 2p region, Si^0, Si^{3+} and Si^{4+} peaks were observed at around 98.7, 101.7, and 102.7 eV, respectively.

The peaks in Li 1s and Si 2p regions remained unchanged until the capacity density for the lithiation reached around 1318 mAh g_{Si}^{-1} (red curves in Figure 4(a) and left panel of Figure 5). It is noted that the intensities of all of the peaks gradually decreased in this capacity range. This can be attributed to the fluctuation of incident photon flux because the shift of Si $2p_{3/2}$ peak attributed to the increase in Li content, was absent. Apart from Li_2CO_3 present from the beginning, Li_2O and Li_4SiO_4, which are expected to attenuate the photoelectron signals from Si, have not yet been detected at this point.

When the capacity density reached around 1482 mAh g_{Si}^{-1} (green curves in Figure 4(a) and left panel of Figure 5), new peaks corresponding to Li_ySi suddenly appeared at 53.0 eV in the Li 1s region and at 96.4 eV in the Si 2p region as well as a Li silicate peak at around 101 eV in the Si 2p region. In addition, Li_2O was also observed at around 54.5 eV in the Li 1s region. Based on the position of Li_ySi peak at 96.4 eV in the Si 2p region, the composition is identified as $Li_{1.97}Si$ using the correlation in Figure S2.[27]

In the capacity density from 1401 to 1560 mAh g_{Si}^{-1} (between green and orange curves in Figure 4(a) and left panel of Figure 5), the intensities of the Li_ySi, Li silicates, and Li_2O increased with decreasing intensities of Si^0, Si^{3+}, and Si^{4+} species in the Si 2p and Li 1s regions while maintaining the position of the Li_ySi peak. When the capacity density reached 2093 mAh g_{Si}^{-1} (light blue curve in Figure 4(a) and left panel of Figure 5), the Si 2p peaks corresponding to the Si^0, Si^{3+}, and Si^{4+} species disappeared completely. Simultaneously, the Li_ySi peak started to shift monotonically from 96.4 to 96.1 eV at the capacity density of 2591 mAh g_{Si}^{-1} (blue curve in Figure 4(a) and left panel of Figure 5), showing the lithiation of $Li_{2.02}Si$ to $Li_{2.53}Si$ (magnified view in Figure S4) based on the correlation in Figure S2[27] in the Supporting Information. In the Li 1s region, the intensity of the Li_2O peak at around 54.7 eV gradually increased when the capacity density exceeded 2185 mAh g_{Si}^{-1} (between light blue and blue curves in Figure 4(a)), probably due to the side reactions of the topmost Li_ySi with residual gases present in the vacuum chamber. In fact, the intensities of Li_ySi and Li_4SiO_4 slightly decreased in the Si 2p region.

https://doi.org/10.1021/acs.jpclett.5c04065
J. Phys. Chem. Lett. 2026, 17, 2181−2190

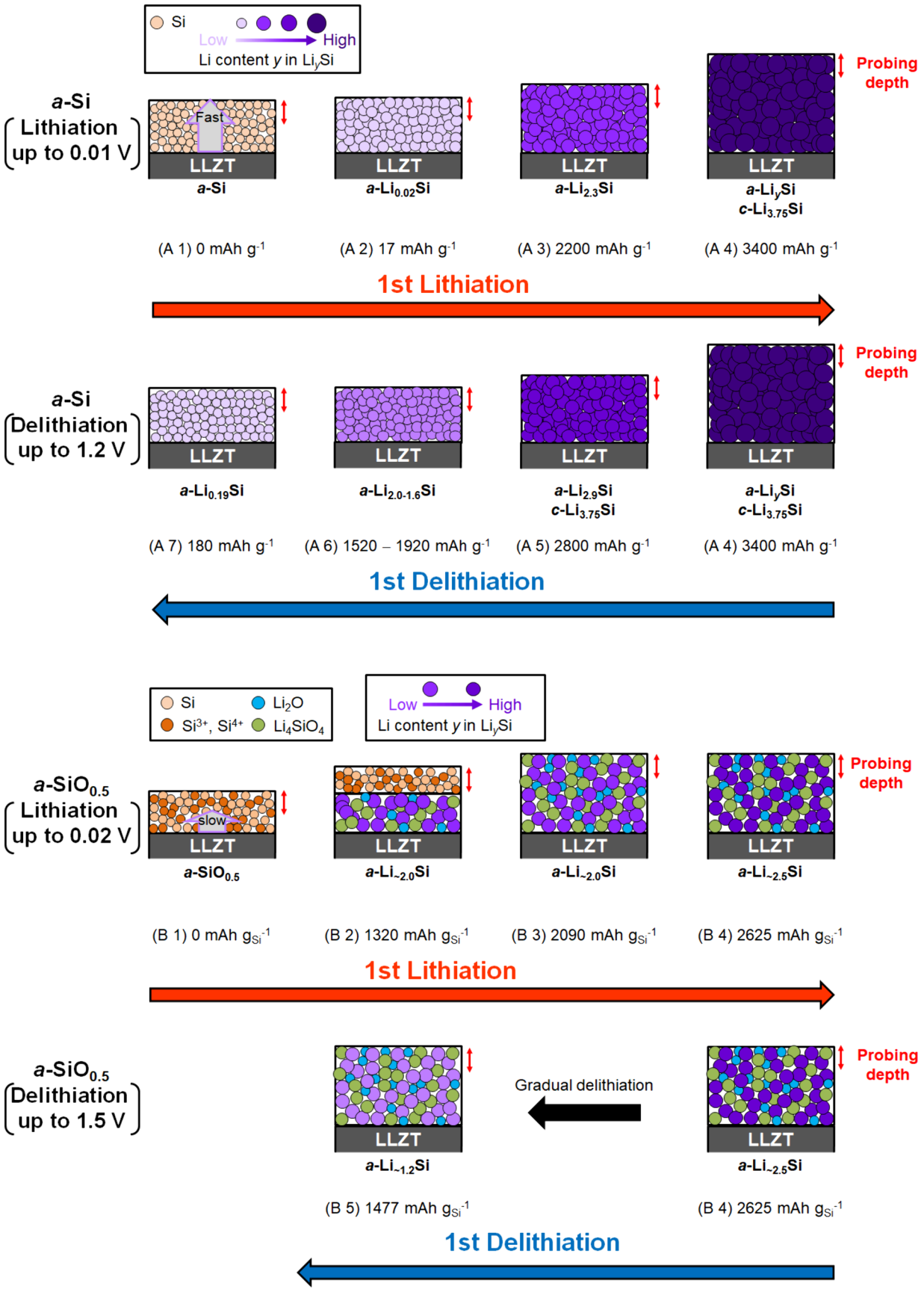

Figure 6. Electrochemical lithiation/delithiation mechanisms of (A) *a*-Si and (B) *a*-$SiO_{0.5}$ thin-film electrodes deposited on the LLZT. (*a* = amorphous; *c* = crystalline).

https://doi.org/10.1021/acs.jpclett.5c04065
J. Phys. Chem. Lett. 2026, 17, 2181−2190

In our previous study on a ∼100 nm thick *a*-Si thin-film electrode, upon lithiation, the position of Si 2p peak drastically shifted from 99.1 to 98.3 eV due to the lithiation of *a*-Si to form slightly lithiated Li_ySi. Even in the first Li 1s spectrum obtained 24 min after initiating the electrochemical lithiation (∼17 mAh g_{Si}^{-1}), Li species were already detected at the *a*-Si surface which is opposite to the Si/LLZT interface. This shows that the lithiation reaction occurred uniformly across the entire *a*-Si thin-film electrode. Then, the Li_ySi peak monotonically shifted to a lower binding energy in response to the electrochemical charge, i.e., Li content *y* in Li_ySi, until it reached 95.4 eV to form $Li_{3.5}Si$.[27] In our present study on the *a*-SiO_x thin-film electrode, however, the Si $2p_{3/2}$ peak remained unchanged until ∼1300 mAh g_{Si}^{-1} and then $Li_{\sim 2.0}Si$ suddenly appeared at ∼1400 mAh g_{Si}^{-1}. This clear contrast suggests that the lithiation proceeded in a layer-by-layer manner due to the relatively low conductivity of SiO_x; in the initial stage, the lithiation of SiO_x occurred at the vicinity of SiO_x/LLZT interface which was located beyond the probing depth of XPS, and then gradually propagated into the bulk and approached the probing depth of XPS as the composition reached $Li_{\sim 2.0}Si$ to elongate an ion conductive pathway.

The $Li_{2.53}Si$ peak started to shift immediately after starting the subsequent delithiation (Figure 4(b) and the right panel of Figure 5). Thereafter, the Li_ySi peak in the Si 2p region monotonically shifted to a higher binding energy up to 97.0 eV equivalent to $Li_{1.20}Si$ based on the correlation in Figure S3, and the intensity of the Li_ySi peak at around 52.8 eV in the Li 1s region gradually decreased. Such a monotonic shift of Li_ySi peak during delithiation was also observed in our previous study after shallow electrochemical lithiation of the *a*-Si thin-film electrode to form $Li_{2.3}Si$.[27] This result suggests that the delithiation reaction occurred uniformly across the *a*-SiO_x thin-film electrode once the ion conductive pathway composed of the Li_ySi was formed in the first lithiation.

It is noteworthy that, in the *a*-Si thin-film electrode examined in our previous study, *a*-$Li_{3.45}Si$ was formed after lithiation up to around 3300 mAh g^{-1} at 0.02 V.[27] In contrast, electrochemical lithiation of the *a*-SiO_x thin-film electrode spontaneously ceased at 2625 mAh g_{Si}^{-1} at 0.02 V, likely due to the presence of highly resistive species. Such a self-limiting property may help prevent excessive lithiation and thereby improve cycle life, as deep lithiation leading to the formation of *c*-$Li_{3.75}Si$ causes rapid capacity fading due to the considerable volume change associated with phase transition to *a*-Li_ySi during the subsequent delithiation.[27]

Figure S5 shows the time course of photoelectron spectra during the second lithiation and delithiation. The peak positions of each chemical species in the Li 1s and Si $2p_{3/2}$ regions were plotted as a function of capacity density as shown in Figure S6. The spectral features related to Li_ySi quasi-reversibly responded to the electrochemical lithiation/delithiation; the intensity of Li_ySi peak at 52.7 eV increased/decreased and the Si $2p_{3/2}$ peak of Li_ySi shifted to a lower/higher binding energy during the lithiation/delithiation, confirming that the lithiation and delithiation uniformly occurred across the *a*-SiO_x thin-film electrode using the ion conductive Li_ySi pathway.

The mechanism of the first electrochemical lithiation/delithiation of the *a*-SiO_x thin-film electrode on a LLZT sheet is shown in Figure 6 together with that of *a*-Si thin-film electrode in our previous study.[27] In the pristine state (A 1), *a*-Si was distributed across the entire thin-film electrode. (A 2) Upon lithiation, *a*-Si was converted into a slightly lithiated *a*-Li_ySi. (A 3, 4) Then, as the capacity density increased, the Li content *y* in Li_ySi increased, and eventually $Li_{3.5}Si$ formed at the capacity of 3400 mAh g^{-1} where *a*-Li_ySi and *c*-$Li_{3.75}Si$ coexisted, based on an assumption that all the electrical charge was consumed for the lithiation. In these processes (A 1−4), the composition of Li_ySi was considered to be uniform throughout the thin-film electrode because of its relatively high ionic conductivity. (A 5) During the subsequent delithiation, Li ions were preferentially extracted from the *a*-Li_ySi. (A 6) In the capacity range 1520−1920 mAh g^{-1} corresponding to the Li content *y* from 2.0 to 1.6, the phase transition from *c*-$Li_{3.75}Si$ to *a*-Li_ySi occurred, as evident by the drastic shift of Li_ySi peak as well as the positive dQ/dV peak around 0.41 V.[27] (A 7) After the phase transition, the Li content *y* gradually decreased as evident by a monotonic shift of the Li_ySi peak.[27]

(B 1) In the pristine state, the *a*-SiO_x thin-film electrode was mainly composed of Si^0, Si^{3+}, and Si^{4+} species. We assume that Si^0 domains were uniformly distributed within the SiO_x thin film as previously reported.[14,21,42] The oxygen content *x* in SiO_x was estimated to be ∼0.5 from the SEM-EDS and HAXPES spectra as shown in Figure S1 in the Supporting Information. (B 2) At the early stage, the lithiation occurred in the vicinity of the SiO_x/LLZT interface which is beyond the probing depth of XPS, to form Li_ySi, Li_2O, and Li_4SiO_4, due to the intrinsically low ionic conductivity of Si oxide species.[22,43−45] (B 3) The lithiation gradually propagated toward the surface opposite to the SiO_x/LLZT interface, while forming an ion conductive pathway composed of $Li_{\sim 2.0}Si$. (B 4) The lithiation reaction eventually reached the surface, which is the subject of XPS measurements, and further lithiation of the $Li_{\sim 2.0}Si$ occurred up to $Li_{\sim 2.5}Si$ until it reached the cut off voltage. (B 5) Delithiation proceeded uniformly across the thin film using the ion conductive Li_ySi pathway.

In summary, electrochemical lithiation/delithiation processes of an *a*-SiO_x thin-film electrode deposited on a LLZT sheet were analyzed using *operando* XPS. Lithiation of SiO_x composed of Si^0, Si^{3+}, and Si^{4+} species first occurred in the vicinity of the SiO_x/LLZT interface to form Li_ySi, Li_2O, and Li_4SiO_4, and then gradually propagated to the opposite surface which is the subject of XPS measurements, to elongate an ion conductive pathway composed of $Li_{\sim 2.0}Si$. After the formation of the pathway, further lithiation into $Li_{\sim 2.0}Si$ occurred to form $Li_{\sim 2.5}Si$. In the subsequent delithiation and cycles thereafter, lithiation/delithiation occurred while maintaining a spatially uniform composition across the *a*-SiO_x thin-film electrode via the pathway. Moreover, the Li content *y* in Li_ySi reversibly responded to electrochemical lithiation/delithiation, as evident by the reversible shift of Si 2p peaks. In the case of *a*-Si thin-film electrode,[27] electrochemical lithiation/delithiation occurred reversibly within the Li content range $y = 0$ to ∼2.3, leading to relatively high capacity retention. Once *c*-$Li_{3.75}Si$ was formed during deeper lithiation up to around 3400 mAh g^{-1}, however, a phase transition from *c*-$Li_{3.75}Si$ to *a*-Li_ySi occurred during the successive delithiation, resulting in rapid capacity fading due to significant volume changes.[27] Unlike, electrochemical lithiation of SiO_x spontaneously ceased at a composition of Li_ySi with lower Li content than that of pure *a*-Si, owing to the formation of highly resistive species such as Li_2O, Li_2CO_3, and Li_4SiO_4. This self-limiting property is expected to help prevent excessive lithiation which may cause rapid capacity loss.

https://doi.org/10.1021/acs.jpclett.5c04065
J. Phys. Chem. Lett. 2026, 17, 2181−2190

■ ASSOCIATED CONTENT

Supporting Information

The Supporting Information is available free of charge at https://pubs.acs.org/doi/10.1021/acs.jpclett.5c04065.

Detailed experimental procedures, oxygen content x in the a-SiO_x thin-film electrode in the pristine state estimated by XPS using an Al Kα source, HAXPES using a Cr Kα source, and SEM-EDS analysis, linear correlation between the position of Li_ySi peaks in Si 2p region and the Li content y during the first lithiation and delithiation of the a-Si thin-film electrode, Li content y in Li_ySi at the end of the first lithiation of the a-SiO_x thin-film electrode estimated from the linear correlation, and photoelectron spectra during the second lithiation and delithiation (PDF)

■ AUTHOR INFORMATION

Corresponding Author

Takuya Masuda − *Research Center for Energy and Environmental Materials (GREEN), National Institute for Materials Science (NIMS), Tsukuba, Ibaraki 305-0044, Japan; Graduate School of Chemical Sciences and Engineering, Hokkaido University, Sapporo, Hokkaido 060-0810, Japan;* orcid.org/0000-0001-7462-2177; Email: MASUDA.Takuya@nims.go.jp

Authors

Tsukasa Iwama − *Research Center for Energy and Environmental Materials (GREEN), National Institute for Materials Science (NIMS), Tsukuba, Ibaraki 305-0044, Japan; Graduate School of Chemical Sciences and Engineering, Hokkaido University, Sapporo, Hokkaido 060-0810, Japan*

Ryosuke Sugimoto − *Department of Molecular Chemistry and Biochemistry, Doshisha University, Kyotanabe, Kyoto 610-0321, Japan*

Raimu Endo − *Research Center for Energy and Environmental Materials (GREEN), National Institute for Materials Science (NIMS), Tsukuba, Ibaraki 305-0044, Japan; Graduate School of Chemical Sciences and Engineering, Hokkaido University, Sapporo, Hokkaido 060-0810, Japan*

Tsuyoshi Ohnishi − *Research Center for Energy and Environmental Materials (GREEN), National Institute for Materials Science (NIMS), Tsukuba, Ibaraki 305-0044, Japan;* orcid.org/0000-0002-2333-7752

Masakazu Haruta − *Department of Electric and Electronic Engineering, Kindai University, Iizuka, Fukuoka 820-8555, Japan*

Takayuki Doi − *Department of Molecular Chemistry and Biochemistry, Doshisha University, Kyotanabe, Kyoto 610-0321, Japan;* orcid.org/0000-0003-1081-9223

Complete contact information is available at: https://pubs.acs.org/10.1021/acs.jpclett.5c04065

Notes

The authors declare no competing financial interest.

■ ACKNOWLEDGMENTS

The present work was supported by JST GteX Program Japan (Grant Nos. JPMJGX23S6, JPMJGX23S2 and JPMJGX23S3), JST COI-NEXT (Grant No. JPMJPF2016) and a grant for the Science on Interfacial Ion Dynamics for Solid State Ionics Devices ("Interface IONICS", Grant No. JP20H05300). The authors acknowledge the NIMS Battery Platform.

■ REFERENCES

(1) Sharma, R. A.; Seefurth, R. N. Thermodynamic Properties of the Lithium-Silicon System. *J. Electrochem. Soc.* **1976**, *123* (12), 1763.

(2) Wen, C. J.; Huggins, R. A. Chemical Diffusion in Intermediate Phases in the Lithium-Silicon System. *J. Solid State Chem.* **1981**, *37*, 271−278.

(3) Obrovac, M. N.; Christensen, L. Structural Changes in Silicon Anodes during Lithium Insertion/Extraction. *Electrochem. Solid-State Lett.* **2004**, *7*, A93−A96.

(4) Hatchard, T. D.; Dahn, J. R. In Situ XRD and Electrochemical Study of the Reaction of Lithium with Amorphous Silicon. *J. Electrochem. Soc.* **2004**, *151*, A838−A842.

(5) van der Marel, C.; Vinke, G. J. B.; van der Lugt, W. The Phase Diagram of the System Lithium-Silicon. *Solid State Commun.* **1985**, *54* (11), 917−919.

(6) Li, J.; Dahn, J. R. An In Situ X-Ray Diffraction Study of the Reaction of Li with Crystalline Si. *J. Electrochem. Soc.* **2007**, *154*, A156.

(7) Nitta, N.; Wu, F.; Lee, J. T.; Yushin, G. Li-ion battery materials: present and future. *Mater. Today* **2015**, *18* (5), 252−264.

(8) Demirkan, M. T.; Trahey, L.; Karabacak, T. Cycling performance of density modulated multilayer silicon thin film anodes in Li-ion batteries. *J. Power Sources* **2015**, *273*, 52−61.

(9) Morino, Y.; Takase, K.; Kanazawa, A.; Nagaoka, N.; Koshitani, N. In-Situ Internal Observation of Silicon Composite Anode in All-Solid-State Battery Using X-ray CT. *ACS Appl. Mater. Interfaces* **2025**, *17* (16), 23786−23794.

(10) Domi, Y.; Usui, H.; Sakaguchi, H. Analysis of the interfacial reaction between Si-based anodes and electrolytes in Li-ion batteries. *Chem. Commun. (Camb)* **2024**, *60* (89), 12986−12999.

(11) Liu, X. H.; Zhong, L.; Huang, S.; Mao, S. X.; Zhu, T.; Huang, J. Y. Size-Dependent Fracture of Silicon Nanoparticles During Lithiation. *ACS Nano* **2012**, *6*, 1522−1531.

(12) Yasuda, K.; Kashitani, Y.; Kizaki, S.; Takeshita, K.; Fujita, T.; Shimosaki, S. Thermodynamic analysis and effect of crystallinity for silicon monoxide negative electrode for lithium ion batteries. *J. Power Sources* **2016**, *329*, 462−472.

(13) Kim, J.-H.; Park, C.-M.; Kim, H.; Kim, Y.-J.; Sohn, H.-J. Electrochemical behavior of SiO anode for Li secondary batteries. *J. Electroanal. Chem.* **2011**, *661* (1), 245−249.

(14) Kim, T.; Park, S.; Oh, S. M. Solid-State NMR and Electrochemical Dilatometry Study on Li^+ Uptake Extraction Mechanism in SiO Electrode. *J. Electrochem. Soc.* **2007**, *154*, A1112.

(15) Guo, B.; Shu, J.; Wang, Z.; Yang, H.; Shi, L.; Liu, Y.; Chen, L. Electrochemical reduction of nano-SiO_2 in hard carbon as anode material for lithium ion batteries. *Electrochem. Commun.* **2008**, *10* (12), 1876−1878.

(16) Haruta, M.; Doi, T.; Inaba, M. Oxygen-Content Dependence of Cycle Performance and Morphology Changes in Amorphous-SiO_x Thin-Film Negative Electrodes for Lithium-Ion Batteries. *J. Electrochem. Soc.* **2019**, *166* (2), A258−A263.

(17) Miyazaki, R.; Ohta, N.; Ohnishi, T.; Takada, K. Anode properties of silicon-rich amorphous silicon suboxide films in all-solid-state lithium batteries. *J. Power Sources* **2016**, *329*, 41−49.

(18) Sugimoto, R.; Marumoto, K.; Haruta, M.; Inaba, M.; Doi, T. Quantitative Evaluation and Improvement of Interfacial Li^+ Transfer Between SiO_x Electrode and Garnet-Type Ta-Doped $Li_7La_3Zr_2O_{12}$ Electrolyte. *ChemElectroChem.* **2022**, *9* (17), No. e202200491.

(19) Kitada, K.; Pecher, O.; Magusin, P. C. M. M.; Groh, M. F.; Weatherup, R. S.; Grey, C. P. Unraveling the Reaction Mechanisms of SiO Anodes for Li-Ion Batteries by Combining *in Situ* ^{7}Li and *ex Situ* ^{7}Li/^{29}Si Solid-State NMR Spectroscopy. *J. Am. Chem. Soc.* **2019**, *141* (17), 7014−7027.

(20) Takezawa, H.; Ito, S.; Yoshizawa, H.; Abe, T. Structural stabilization on SiO_x film anode with large areal capacity for enhanced cyclability in lithium-ion batteries. *J. Power Sources* **2016**, *324*, 45−51.
(21) Choi, G.; Kim, J.; Kang, B. Understanding Limited Reversible Capacity of a SiO Electrode during the First Cycle and Its Effect on Initial Coulombic Efficiency. *Chem. Mater.* **2019**, *31* (16), 6097−6104.
(22) Jung, S. C.; Kim, H.-J.; Kim, J.-H.; Han, Y.-K. Atomic-Level Understanding toward a High-Capacity and High-Power Silicon Oxide (SiO) Material. *J. Phys. Chem. C* **2016**, *120* (2), 886−892.
(23) Nguyen, C. C.; Choi, H.; Song, S.-W. Roles of Oxygen and Interfacial Stabilization in Enhancing the Cycling Ability of Silicon Oxide Anodes for Rechargeable Lithium Batteries. *J. Electrochem. Soc.* **2013**, *160* (6), A906−A914.
(24) Xie, G.; Tan, X.; Shi, Z.; Peng, Y.; Ma, Y.; Zhong, Y.; Wang, F.; He, J.; Zhu, Z.; Cheng, X. B. SiO_x Based Anodes for Advanced Li-Ion Batteries: Recent Progress and Perspectives. *Adv. Funct. Mater.* **2025**, *35* (6), 2414714.
(25) Kim, T.; Li, H.; Gervasone, R.; Kim, J. M.; Lee, J. Y. Review on Improving the Performance of SiO_x Anodes for a Lithium-Ion Battery through Insertion of Heteroatoms: State of the Art and Outlook. *Energy Fuels* **2023**, *37* (18), 13563−13578.
(26) Cho, J. H.; Xiao, X.; Verbrugge, M. W.; Sheldon, B. W. Influence of Oxygen Content on the Structural Evolution of SiOx Thin-Film Electrodes with Subsequent Lithiation/Delithiation Cycles. *ACS Appl. Energy Mater.* **2022**, *5* (11), 13293−13306.
(27) Endo, R.; Ohnishi, T.; Takada, K.; Masuda, T. Electrochemical Lithiation and Delithiation in Amorphous Si Thin Film Electrodes Studied by Operando X-ray Photoelectron Spectroscopy. *J. Phys. Chem. Lett.* **2022**, *13* (31), 7363−7370.
(28) Endo, R.; Ohnishi, T.; Takada, K.; Masuda, T. Instrumentation for tracking electrochemical reactions by x-ray photoelectron spectroscopy under conventional vacuum conditions. *J. Phys. Commun.* **2021**, *5* (1), 015001.
(29) Endo, R.; Ohnishi, T.; Takada, K.; Masuda, T. *In Situ* Observation of Lithiation and Delithiation Reactions of a Silicon Thin Film Electrode for All-Solid-State Lithium-Ion Batteries by X-ray Photoelectron Spectroscopy. *J. Phys. Chem. Lett.* **2020**, *11* (16), 6649−6654.
(30) Maranchi, J. P.; Hepp, A. F.; Kumta, P. N. High Capacity, Reversible Silicon Thin-Film Anodes for Lithium-Ion Batteries. *Electrochem. Solid-State Lett.* **2003**, *6*, A198−A201.
(31) Ohara, S.; Suzuki, J.; Sekine, K.; Takamura, T. A thin film silicon anode for Li-ion batteries having a very large specific capacity and long cycle life. *J. Power Sources* **2004**, *136* (2), 303−306.
(32) Ohta, N.; Kimura, S.; Sakabe, J.; Mitsuishi, K.; Ohnishi, T.; Takada, K. Anode Properties of Si Nanoparticles in All-Solid-State Li Batteries. *ACS Appl. Energy Mater.* **2019**, *2* (10), 7005−7008.
(33) Cras, F. L.; Pecquenard, B.; Dubois, V.; Phan, V.-P.; Guy-Bouyssou, D. All-Solid-State Lithium-Ion Microbatteries Using Silicon Nanofilm Anodes: High Performance and Memory Effect. *Adv. Energy Mater.* **2015**, *5* (19), 1501061.
(34) Schmid, M.; Steinrück, H.-P.; Gottfried, J. M. A new asymmetric Pseudo-Voigt function for more efficient fitting of XPS lines. *Surf. Interface Anal.* **2014**, *46* (8), 505−511.
(35) Alfonsetti, R.; De Simone, G.; Lozzi, L.; Passacantando, M.; Picozzi, P.; Santucci, S. SiO_x surface stoichiometry by XPS: A comparison of various methods. *Surf. Interface Anal.* **1994**, *22* (1−12), 89−92.
(36) Bell, F. G.; Ley, L. Photoemission study of SiO_x ($0 \leq x \leq 2$) alloys. *Phys. Rev. B* **1988**, *37* (14), 8383−8393.
(37) Jensen, D. S.; Kanyal, S. S.; Madaan, N.; Vail, M. A.; Dadson, A. E.; Engelhard, M. H.; Linford, M. R. Silicon (100)/SiO_2 by XPS. *Surf. Sci. Spectra* **2013**, *20* (1), 36−42.
(38) Kanamura, K.; Takezawa, H.; Shiraishi, S.; Takehara, Z. Chemical Reaction of Lithium Surface during Immersion in $LiClO_4$ or $LiPF_6$/DEC Electrolyte. *J. Electrochem. Soc.* **1997**, *144*, 1900−1906.
(39) Philippe, B.; Dedryvère, R.; Allouche, J.; Lindgren, F.; Gorgoi, M.; Rensmo, H.; Gonbeau, D.; Edström, K. Nanosilicon Electrodes for Lithium-Ion Batteries: Interfacial Mechanisms Studied by Hard and Soft X-ray Photoelectron Spectroscopy. *Chem. Mater.* **2012**, *24* (6), 1107−1115.
(40) Takezawa, H.; Iwamoto, K.; Ito, S.; Yoshizawa, H. Electrochemical behaviors of nonstoichiometric silicon suboxides (SiO_x) film prepared by reactive evaporation for lithium rechargeable batteries. *J. Power Sources* **2013**, *244*, 149−157.
(41) Cao, C.; Abate, I. I.; Sivonxay, E.; Shyam, B.; Jia, C.; Moritz, B.; Devereaux, T. P.; Persson, K. A.; Steinrück, H.-G.; Toney, M. F. Solid Electrolyte Interphase on Native Oxide-Terminated Silicon Anodes for Li-Ion Batteries. *Joule* **2019**, *3* (3), 762−781.
(42) Hirata, A.; Kohara, S.; Asada, T.; Arao, M.; Yogi, C.; Imai, H.; Tan, Y.; Fujita, T.; Chen, M. Atomic-scale disproportionation in amorphous silicon monoxide. *Nat. Commun.* **2016**, *7* (1), 11591.
(43) Xun, S.; Song, X.; Wang, L.; Grass, M. E.; Liu, Z.; Battaglia, V. S.; Liu, G. The Effects of Native Oxide Surface Layer on the Electrochemical Performance of Si Nanoparticle-Based Electrodes. *J. Electrochem. Soc.* **2011**, *158* (12), A1260−A1266.
(44) Sivonxay, E.; Aykol, M.; Persson, K. A. The lithiation process and Li diffusion in amorphous SiO_2 and Si from first-principles. *Electrochim. Acta* **2020**, *331*, 135344.
(45) Tang, C.; Liu, Y.; Xu, C.; Zhu, J.; Wei, X.; Zhou, L.; He, L.; Yang, W.; Mai, L. Ultrafine Nickel-Nanoparticle-Enabled SiO_2 Hierarchical Hollow Spheres for High-Performance Lithium Storage. *Adv. Funct. Mater.* **2018**, *28* (3), 1704561.

https://doi.org/10.1021/acs.jpclett.5c04065
J. Phys. Chem. Lett. 2026, 17, 2181−2190